Influence of Sample Preparation, Temperature, Light, and Pressure on the Two-Step Spin Crossover Mononuclear Compound [Fe(bapbpy)(NCS)$_2$]

Sylvestre Bonnet,[†] Gábor Molnár,[‡,§] José Sanchez Costa,[†] Maxime A. Siegler,[||] Anthony L. Spek,[||] Azedine Bousseksou,[‡,§] Wen-Tian Fu,[†] Patrick Gamez,[†] and Jan Reedijk*[,†]

Leiden Institute of Chemistry, Leiden University, P.O. Box 9502, 2300 RA Leiden, The Netherlands, Laboratoire de Chimie de Coordination, CNRS, 205 Route de Narbonne, 31077 Toulouse, France, Université de Toulouse, UPS, INPT, LCC, F-31077 Toulouse, France, and Bijvoet Center for Biomolecular Research Crystal and Structural Chemistry, Utrecht University, Padualaan 8, 3584 CH Utrecht, The Netherlands

Received December 18, 2008. Revised Manuscript Received January 16, 2009

The three phases of the mononuclear two-step spin crossover compound [Fe(bapbpy)(NCS)$_2$] (**1**) are characterized by powder X-ray diffraction, Mössbauer spectroscopy, Raman spectroscopy, calorimetry, and magnetic susceptibility measurements. Mössbauer and Raman spectroscopies confirm the results obtained from previous single crystal X-ray diffraction studies, as they show that the intermediate phase is characterized by a 1:2 high-spin/low-spin ratio and that it is not a mixture of the high-spin state (HS) and low-spin state (LS) phases. Sample preparation and sample history studies show that the spin crossover (SCO) properties of this compound are quite robust, as the two steps and hysteresis cycles are present both in the powder and in recrystallized samples and conserved when the sample is cooled and heated several times. Compound **2**, a DMF solvate having the formula [Fe(bapbpy)(NCS)$_2$]·2DMF, shows SCO properties but no cooperative effects. The origin of the strong cooperativity found in compound **1** is discussed. Finally, external perturbations have been applied to compound **1**. First, light irradiation at low temperatures promotes the LS → HS transition with reasonably good optical conversions [∼70%, T(LIESST) = 56 K]. Second, the application of hydrostatic pressure increases both the temperature and the hysteresis width of the higher-temperature transition (HS ↔ IP), while unexpectedly suppressing the lower-temperature transition (IP ↔ LS).

Introduction

Spin crossover (SCO) materials are very appealing because they represent one of the best examples of molecular switching.[1−3] Although ligand design does play a major role in the discovery of new SCO systems, it is increasingly realized that the magnetic properties of SCO materials also depend on intermolecular interactions found in the solid state, which are hardly predictable. As a result, extensive studies should be carried out for each new SCO compound to deepen the overall understanding of the structure−property relationship for this type of material. In particular, cooperative effects, which lead to steep transitions and hysteresis loops, are important to study. It is known that the combinations of two bidentate *N*,*N*-bis(2-pyridyl)amine ligands and two monodentate ligands enable iron(II) SCO complexes to be obtained.[4,5] In a recent communication,[6] we reported the synthesis of the new tetradentate ligand bapbpy, which contains two fused *N*,*N*-bis(2-pyridyl)amines. Coordination of bapbpy to [Fe(NCS)$_2$] leads to the mononuclear two-step SCO compound [Fe(bapbpy)(NCS)$_2$] (**1**) (see Scheme 1). In this compound, remarkable cooperative behaviors are observed, resulting not only in the two steps but also in steep transition curves and two hysteresis loops.

Scheme 1. Molecular Structures of bapbpy and Compound 1

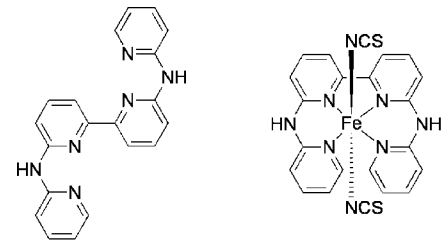

bapbpy **1** trans-[Fe(bapbpy)(NCS)$_2$]

In our preliminary report,[6] temperature-dependent magnetic susceptibility measurements, single-crystal X-ray structure determinations, and differential scanning calorimetry (hereafter, DSC) showed evidence of three phases for compound **1**: a high-spin phase (phase **I**), an intermediate phase stable over a wide temperature range (phase **II**), and a low-spin phase (phase **III**). In the intermediate phase (hereafter, IP), two-thirds of the iron(II) centers are found

* Corresponding author. E-mail: reedijk@chem.leidenuniv.nl. Fax: (+31) 71-5274671. Tel: (+31) 71-5274459.
[†] Leiden University.
[‡] CNRS.
[§] Université de Toulouse.
[||] Utrecht University.

(1) Gütlich, P. *Angew. Chem., Int. Ed.* **1994**, *33*, 2024.
(2) Gütlich, P.; Goodwin, H. A. *Spin CrossOver in Transition Metal Compounds*; Topics in Current Chemestry; Springer: Berlin, Germany, 2004; Vols. *I*−*III*.
(3) Kahn, O. *Curr. Opin. Solid State Mater. Sci.* **1996**, *1*, 547.

10.1021/cm803414q CCC: $40.75
Published on Web 02/16/2009

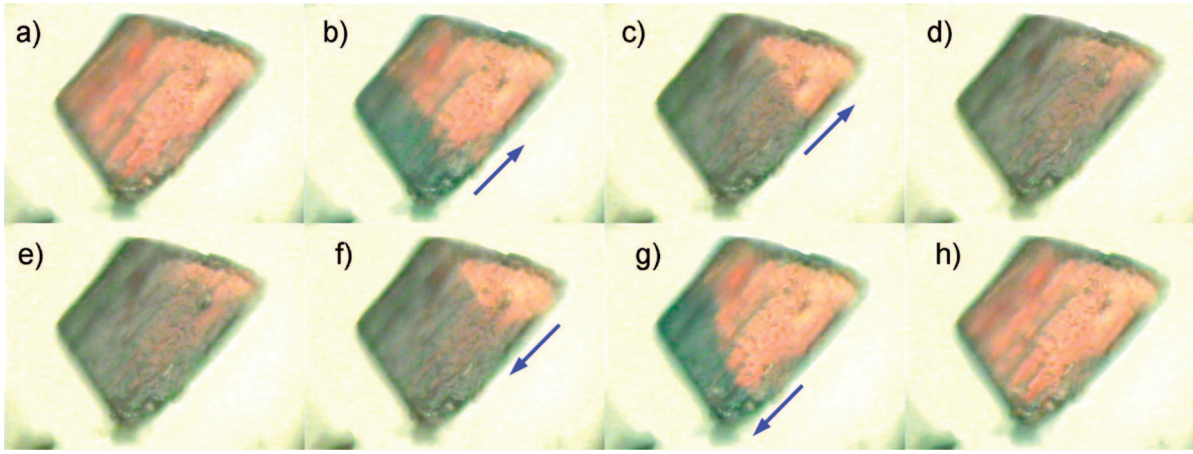

Figure 1. Optical microscopy digital photographs of one single crystal of **1**, which undergoes the cooling spin transition **I** → **II** (a−d, ∼235 K, cooling rate −2 K·min^{-1}; $t_a = 0$, $t_b = 3$ s, $t_c = 7$ s; $t_d = 10$ s) and the heating spin transition **II** → **I** (e−h, ∼238 K, heating rate +2 K·min^{-1}; $t_e = 0$, $t_f = 9$ s, $t_g = 12$ s; $t_h = 14$ s). The blue arrows indicate the direction of propagation of the front observed during the reversible transitions **I** ↔ **II**. The picture size is 130 μm × 100 μm.

in the low-spin state (LS), whereas one-third remains in the high-spin state (HS). All techniques confirm that both solid−solid phase transitions **I** ↔ **II** and **II** ↔ **III** are first order and reversible. These properties are corroborated by the occurrence of steep transition curves, hysteresis cycles, discontinuities in *V*/*Z* (i.e., the volume per formula unit), and large ΔH at both transition points. The crystal structures of the three phases show H-bonding and $\pi-\pi$ stacking interactions along [001] that may be responsible for the strong cooperative effects observed in this compound. Systems, for which an ordered IP was found, are scarce.[7−9] Remarkably, the IP of compound **1** remains ordered and is characterized by the unprecedented [HS−LS−LS] motif found along [001].

In the present article we discuss important additional experimental data for compound **1**, aimed at a better understanding of its peculiar cooperative behavior. In the first place, optical microscopy on a single crystal of **1** allowed the direct observation of the higher-temperature spin transition (i.e., the transition **I** ↔ **II**). Second, the influence of sample preparation on the SCO behavior of compound **1** has been examined in detail. Single crystals of the related compound **2**, a *N*,*N*-dimethylformamide (DMF) solvate of **1** with a ratio **1**:DMF of 1:2, have been synthesized for that purpose. H-bond interactions of the DMF molecules with the metal complex are observed in the crystal structure of **2**, concomitant with a strong alteration of its SCO properties, which suggests the involvement of H-bonding interactions (and also $\pi-\pi$ stacking interactions) in the cooperative behavior of compound **1**. In a third part, powder X-ray diffraction and Mössbauer and Raman spectroscopic studies have been performed on compound **1**, leading to a more complete view, notably, on the nature of the IP. In the last part, the effects of light irradiation and hydrostatic pressure on the properties of compound **1** are presented.

Results

Optical Microscopy. Optical microscopy is a valuable technique to study phase transitions: first, it can reveal thermal events that are not discernible by DSC; second, one can observe the coexistence of two phases near the transition temperature.[9] During SCO, the change in electron configuration of the iron(II) center ($^1A_1 \leftrightarrows {}^5T_2$) is generally accompanied by a color change of the material.[10] For the two-step SCO compound **1**, only the first spin transition (**I** ↔ **II**) can be observed via optical microscopy, as the initial light red color of a single crystal of **1** (phase **I**, HS) turns to dark red (phase **II**, IP).[11] Several single crystals were cooled and heated under a nitrogen stream between 233 and 243 K at ±2 K·min^{-1}, and their color change was observed under the microscope (see Figure 1 and movie in Supporting Information). In both cooling and heating modes, the color change propagates as a front along the longest dimension of the crystal, until the transition **I** ↔ **II** is completed. The transition front appears near 235 K (cooling mode, **I** → **II**) and near 238 K (heating mode, **II** → **I**) with an estimated hysteresis width of about 3 K in agreement with the magnetic behavior (see the next paragraph). In both modes, the transition front takes a few seconds to propagate always along the longest dimensions of the crystals.[12]

Influence of Sample Preparation on the Spin Transition. The detailed spin-transition properties of compound **1** depend on sample preparation. Three types of samples have been studied: (a) the crude powder (i.e., a mass of microscopic crystalline particles with varying orientations) obtained directly after synthesis; (b) a polycrystalline sample (i.e., an ensemble of single crystals with varying orientations) prepared by recrystallization of the crude powder from DMF/methanol; and (c) a polycrystalline sample prepared by recrystallization of the crude powder from DMF/diisopropylether. The SCO behaviors of the samples (a), (b), and

(4) Quesada, M.; de Hoog, P.; Gamez, P.; Roubeau, O.; Aromi, G.; Donnadieu, B.; Massera, C.; Lutz, M.; Spek, A. L.; Reedijk, J. *Eur. J. Inorg. Chem.* **2006**, 1353.
(5) Quesada, M.; de la Pena-O'Shea, V. A.; Aromi, G.; Geremia, S.; Massera, C.; Roubeau, O.; Gamez, P.; Reedijk, J. *Adv. Mater.* **2007**, *19*, 1397.
(6) Bonnet, S.; Siegler, M. A.; Sanchez Costa, J.; Molnar, G.; Bousseksou, A.; Spek, A. L.; Gamez, P.; Reedijk, J. *Chem. Commun.* **2008**, 5619.
(7) Chernyshov, D.; Hostettler, M.; Tornroos, K. W.; Burgi, H. B. *Angew. Chem., Int. Ed.* **2003**, *42*, 3825.
(8) Klingele, M. H.; Moubaraki, B.; Cashion, J. D.; Murray, K. S.; Brooker, S. *Chem. Commun.* **2005**, 987.
(9) Herbstein, F. H. *Acta Crystallogr.* **2006**, *B62*, 341.

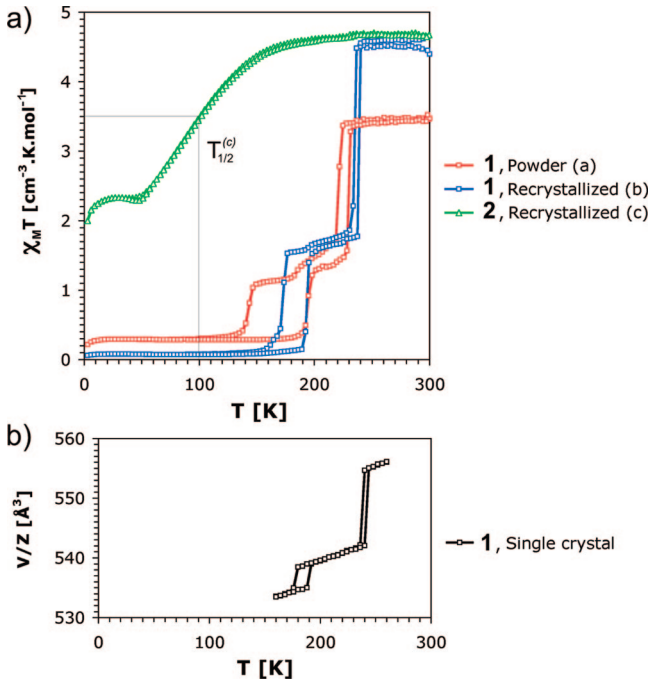

Figure 2. Influence of sample preparation on the SCO of [Fe(bapbpy)(NCS)$_2$]: (a) probed by magnetic susceptibility measurements [cooling/heating rates: ±1.0(1) K·min^{-1}]; (b) probed by the temperature dependence of *V*/*Z* measured via single-crystal X-ray diffraction [±2.0(1) K·min^{-1}].

Table 1. Transition Temperatures and Hysteresis Widths of a Powder, Recrystallized, and Solvated Sample of [Fe(bapbpy)(NCS)$_2$]

sample type	$T^1_c\downarrow$ (K)	$T^1_c\uparrow$ (K)	ΔT^1_{hyst} (K)	$T^2_c\downarrow$ (K)	$T^2_c\uparrow$ (K)	ΔT^2_{hyst} (K)
1, powder (a)	221(1)	231(1)	10(1)	142(1)	196(1)	54(1)
1, recrystallized (b)	235(1)	239(1)	4(1)	172(1)	194(1)	22(1)
2, recrystallized (c)	100(2)	100(2)	0(3)			
1, single crystal[a]	238(2)	242(2)	4(3)	178(2)	190(2)	12(3)

[a] The transition temperatures are derived from the temperature variation of the unit cell volume per formula unit *V*/*Z*, as measured by X-ray diffraction on a single crystal taken from sample (b) (see ref 6).

(c) were examined by $\chi_M T = f(T)$ measurements (χ_M is the molar magnetic susceptibility, T the temperature) in a SQUID magnetometer in both cooling and heating modes (see Figure 2a; cooling and heating rate: ±1 K·min^{-1}). For comparison, the change in the unit cell volume per formula unit *V*/*Z* versus T for one single crystal taken from sample (b) is given in Figure 2b (see our preliminary communication;[6] for a cooling and heating rate of ±2 K·min^{-1}). As shown in Figure 2, the transition temperatures and hysteresis widths for samples (a) and (b) are different (see Table 1), although both samples exhibit a comparable two-step SCO behavior (i.e., with steep transitions curves and hysteresis loops for both transitions). The measurements obtained from single-crystal X-ray diffraction gave slightly different results as well. The higher-temperature transition (**I** → **II** or **II** → **I**) occurs at higher temperature for sample (b) than for sample (a); the hysteresis widths are larger for sample (a) and smaller for sample (b). Those widths are larger than that measured on one single crystal. It should be noted here that the transition temperatures of a first-order phase transition can be defined only for a large ensemble of particles since individual crystals with different size, shape, and defects will display somewhat differing transition temperatures. Regarding the lower-temperature transition (**II** → **III** or **III** → **II**), the transition temperature in the cooling mode ($T^2_c\downarrow$) appears to be highly dependent on the sample preparation, whereas that in the heating mode ($T^2_c\uparrow$) seems to be less affected.

The DSC traces (Figure 3) show also significant differences between samples (a) and (b) (T-range: 100−300 K. The higher-temperature transitions **I** → **II** (cooling rate: −10 K·min^{-1}) and **II** → **I** (heating rate: +10 K·min^{-1}), which are observed for the polycrystalline sample [i.e., sample (b)] near 230 and 240 K, respectively, occur for the powder sample [i.e., sample (a)] near 211 and 220 K, respectively. The lower-temperature transitions **II** → **III** (cooling rate: −10 K·min^{-1}) and **III** → **II** (heating rate: +10 K·min^{-1}) are observed for sample (b) near 169 and 193 K, respectively, but only the latter transition is measurable near 189 K for sample (a) (probably due to the technical limitations of our calorimeter).

The measured macroscopic quantities ΔH and ΔS are estimated to be 10(1) kJ·mol^{-1} and 48(6) J·K^{-1}·mol^{-1} for the transition **I** ↔ **II** of sample (a), whereas it is 17(2) kJ·mol^{-1} and 72(8) J·K^{-1}·mol^{-1} with sample (b).[13] For the transition **III** → **II**, ΔH could not be reliably measured for sample (a), whereas it is 9.7(5) kJ·mol^{-1} for sample (b) (measured at the same cooling/heating rates).[6] The differences observed for the enthalpies of samples (a) and (b) appeared to be rather large; we repeated the DSC measurements on both samples after six months, which produced identical results. As the cooling/heating rates are the same and the mass of the samples are comparable, it is most likely that the different natures of the samples might be responsible for their different calorimetric behaviors.

For sample (c), that is, compound **2**, the magnetic behavior, as measured by magnetic susceptibility measurements, is very different: a gradual HS ↔ LS transition occurs between 200 and 50 K: the value of $\chi_M T$ is 4.70 cm^3·K·mol^{-1} at room temperature and 2.35 cm^3·K·mol^{-1} at 48 K. The temperature corresponding to the HS → LS transition of approximately one-half of the iron(II) centers, that is, $T^{(c)}_{1/2}$, is found near 100(2) K. It is much lower than the average transition temperature for the first transition of compound **1** [T^1_c = 237(1) K]. The value of $\chi_M T$ for compound **2** is stable from 48 K down to 20 K probably because of very slow kinetics of the transition in this temperature range (quenching), but it starts to decrease again due to the zero-field splitting for the residual HS molecules. The high value of $\chi_M T$ found at room temperature for samples (b) and (c) is larger than the spin-only value calculated for a $^5T_2$ ground-state (S = 2) described in an octahedral coordination environment ($\chi_M T$ = 3.0 cm^3·mol^{-1}·K for a g-value equal to 2). Such an

(10) Létard, J. F.; Guionneau, P.; Goux-Capes, L. *Top. Curr. Chem.* **2004**, *235*, 221.
(11) The differences in color between phases **II** (IP) and **III** (LS) are too small to follow the low-temperature transition by optical microscopy.
(12) The front direction probably corresponds to the *c* direction (i.e., the direction of the 1-D supramolecular chains). The faces found at the edges of the longest dimension of the crystal were difficult to index since their indices seemed to vary. Near room temperature, these faces were approximately (10$\bar{4}$) and ($\bar{1}$04) but should have been (10$\bar{2}$) and ($\bar{1}$02) since the normal to these planes is found nearly along the *c* direction.

(13) Given per metal ion involved in the transition.

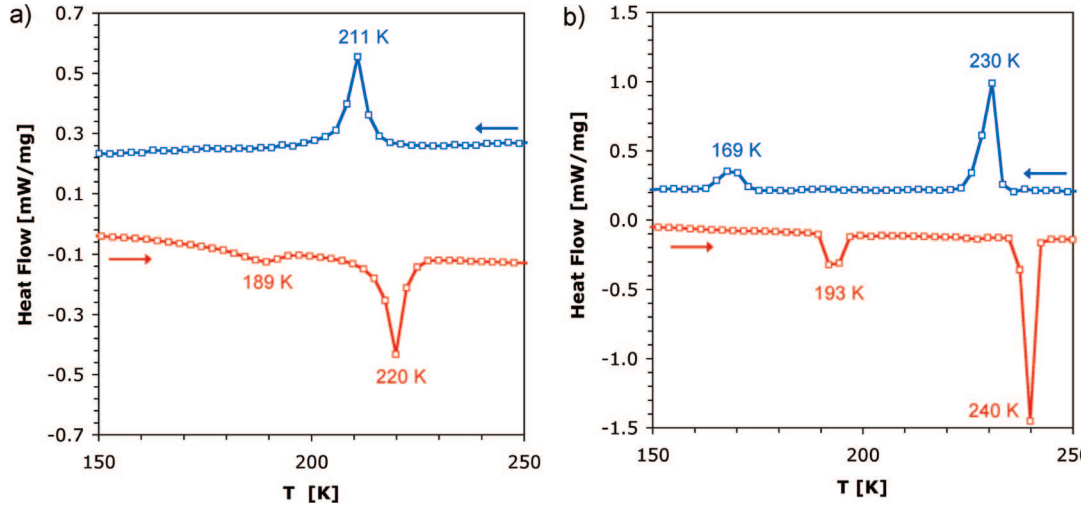

Figure 3. (a) DSC traces for a powder sample [sample (a)] of compound **1**. (b) DSC traces for a polycrystalline [sample (b)] of compound **1**. The traces measured in the cooling and heating modes are colored in blue and red, respectively. Cooling/heating rates: ±10 K·min^{-1}.

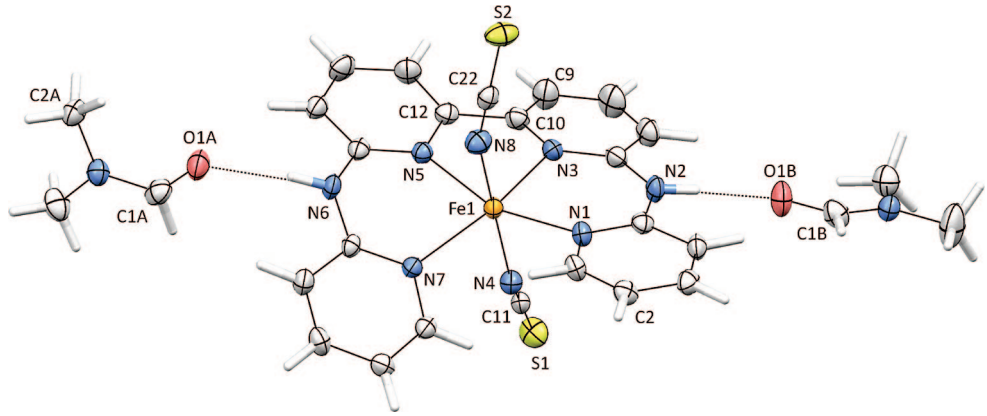

Figure 4. Displacement ellipsoid plot (50% probability level) of the asymmetric unit of [Fe(bapbpy)(NCS)$_2$]·2DMF (compound **2**) at 150(2) K. The N−H···O hydrogen bonds are shown as black dotted lines. The C−H···O and C−H···S contacts are not shown for the sake of clarity.

unusually high $\chi_M T$ value has been also observed for the magnetic susceptibility study of the well-known compound [Fe(ptz)$_6$](BF$_4$)$_2$ (ptz = 1-propyltetrazole).[14] This phenomenon is explained by orientational effects of a crystalline sample which will result in effective magnetic moments that do not correspond to the real average magnetic moments.[15] For the powder sample (a) a value of 3.5 cm^3·mol^{-1}·K is found at room temperature, which is typical for a HS iron(II) center in an octahedral Fe^{II}N$_6$ environment.

When a crushed polycrystalline sample of type (c), that is, compound **2**, is examined via infrared spectroscopy, the recorded IR spectrum shows three intense absorption bands at 1661.7, 1651.8, and 1645.5 cm^{-1}, which are not present in the infrared spectra of samples (a) or (b). These absorption bands are most likely due to the existence of DMF molecules inserted in the crystal lattice of the recrystallized material. The crystal structure of sample (c), determined at 150 K via single crystal X-ray diffraction (see Figure 4, Tables 2 and 3, and Experimental Part), supports the data collected via infrared spectroscopy. Compound **2** [sample (c)] is also mononuclear and shows overall the same coordination environment as compound **1**: the bapbpy ligand coordinates the basal plane of a distorted iron(II) octahedron, with two

Table 2. Crystallographic Data for 2

	2
formula	$C_{22}H_{16}FeN_8S_2$·2(C_3H_7NO)
fw	658.59
cryst syst	triclinic
space group	$P\bar{1}$
T, K	150 (2)
a, b, c, Å	8.8298 (8), 12.2817 (4), 14.3159 (5)
α, β, γ, deg	91.086 (2), 103.967 (2), 95.266 (2)
V, Å^3	1498.87 (15)
Z	2
D_x, Mg m^{-3}	1.459
μ, mm^{-1}	0.69
crystal form, color	thick plate, red
crystal size, mm	0.15 × 0.13 × 0.07
T_{min}, T_{max}	0.834, 0.954
meas reflns	32805
indep reflns	6883
$I > 2\sigma(I)$ reflns	5064
R_{int}	0.047
θ_{max}, deg	27.5
$R[F^2 > 2\sigma(F^2)]$, $wR(F^2)$, S	0.046
$wR(F^2)$	0.093
S	1.19
refined params	398
$(\Delta/\sigma)_{max}$	0.001
$\Delta\rho_{max}$, $\Delta\rho_{min}$, e Å^{-3}	0.46, −0.34

(14) Decurtins, S.; Gütlich, P.; Hasselbach, K. M.; Hauser, A.; Spiering, H. *Inorg. Chem.* **1985**, *24*, 2174.
(15) Both recrystallized samples (b) and (c) show comparable high values at room temperature.

Table 3. Characteristic Bond Distances and Bond Angles for [Fe(bapbpy)(SCN)$_2$]·2DMF (Compound 2) at 150 K

	bond distance [Å]		angles and torsion angles (deg)
Fe1−N1	2.148(2)	N1−Fe1−N3	86.65(9)
Fe1−N3	2.151(2)	N5−Fe1−N7	84.93(8)
Fe1−N4	2.175(3)	N3−Fe1−N5	77.69(9)
Fe1−N5	2.142(2)	N4−Fe1−N3	82.11(9)
Fe1−N7	2.153(2)	N8−Fe1−N5	86.98(9)
Fe1−N6	2.129(3)	N4−Fe1−N8	174.80(10)
N6···O1A	2.830(3)	C11−N4−Fe1	157.0(2)
N2···O1B	2.777(3)	C22−N8−Fe1	157.8(2)
C1A−O1A	1.237(4)	N1···N3···N5···N7	−18.36(11)
C1B−O1B	1.223(4)	N3−C10−C12−N5	−14.5(4)

trans-coordinated thiocyanate ligands and two uncoordinated DMF molecules. However, in this structure the two DMF molecules act as hydrogen bond acceptors via relatively strong N−H···O [N2···O1B = 2.777(3) Å, N6···O1A = 2.830(3) Å] hydrogen bonding interactions with the two N−H donor groups of the bapbpy ligand. Because of these N−H···O hydrogen bonds, the weak N−H···S hydrogen bonds and $\pi-\pi$ stacking interactions observed along [001] in the crystal structures of phases **I**, **II**, and **III** of compound **1** are no longer present in compound **2**. In the crystal structure of **2**, the packing is built from one-dimensional (hereafter, 1-D) chains with the repetitive motif DMF···**1**···DMF along [110]. These chains are stabilized via the stronger N−H···O interactions (i.e., **1**···DMF, see above) together with the weak C−H···O contacts [i.e., DMF···DMF, C2A···O1B = 3.427(4) Å]. Other intermolecular contacts such as the weak C−H···S contacts [C2···S1 = 3.695(4) Å, C9···S2 = 3.604(4) Å] may help as well to stabilize adjacent 1-D chains. In the structure of compound **2** at 150 K, the Fe−N bond distances are typical for a HS iron(II) center.

Influence of Sample History. To study the effects of sample history, the cooling/heating cycles have been repeated six times on the same polycrystalline sample (b) in the magnetometer. These measurements were carried out at slightly different cooling/heating rates to investigate the influence of the cooling/heating rates on the transition temperatures (cooling rates: −0.66 to −1.08 K·min^{-1}, heating rates: +0.68 to 1.12 K·min^{-1}). As shown in Figure 5, the transition temperatures and hysteresis widths remain the same for the six cycles. However, the values of $\chi_M T$ of the HS and IP slightly increase after each cycle during the first cycles (10% of total variation of $\chi_M T$ at room temperature after six cycles) to become stable following approximately four cycles. This phenomenon is often observed when measuring the magnetic properties of polycrystalline samples and can be related to the changes in orientation of the grains due to temperature variations. In the case of SCO compounds, this effect is even more common due to the sensitivity of this phenomenon to any structural changes (e.g., cracking, departure of solvent, etc.) in the crystal lattice.[16,17]

Powder X-ray Diffraction. We previously determined, from the single-crystal X-ray diffraction data, the structures

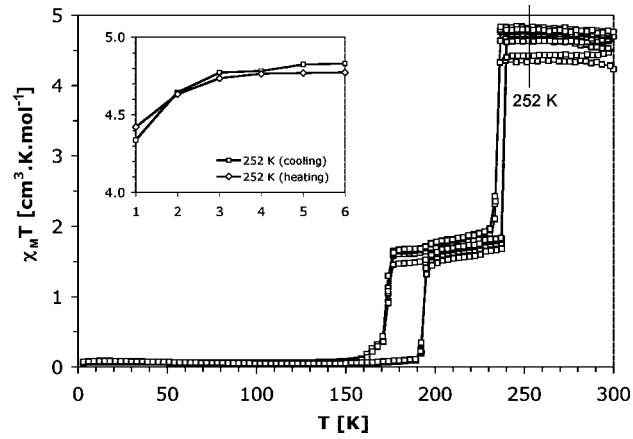

Figure 5. Cycling the spin transitions of one sample (b) of compound **1** by repeating cooling from 300 to 3 K and heating from to 3 to 300 K at different rates (cooling rates: −1.01, −0.92, −0.83, −0.71, −1.08, −0.66 K·min^{-1}; heating rates: 1.05, 0.92, 0.84, 0.73, 1.12, 0.68 K·min^{-1} for cycles 1−6, respectively).

of the three phases **I**, **II**, and **III** of compound **1**, as well as the temperature dependences of the cell parameters.[6] However, X-ray diffraction carried out on one single crystal after recrystallization [sample (b)] may not represent the bulk sample and, consequently, cannot provide sufficient information about subtle heterogeneities found in the sample material. In addition, although magnetic susceptibility measurements give similar behavior for samples (a) and (b), DSC analysis on the powder [sample (a)] reveals noticeable differences compared to the recrystallized sample [type (b)].

Therefore, a powder X-ray diffraction study at low temperature was carried out on sample (a) to determine whether the phase transitions observed on single crystals can be generalized to a bulk powder sample of compound **1**. All data were collected in the cooling mode with a cooling rate of 10 K·min^{-1}. Before each measurement the sample was kept at the specific temperature for 15 min to ensure the thermal equilibrium. Figure 6 shows a portion of the powder X-ray diffraction pattern of sample (a) at three representative temperatures.

At room temperature, the observed diffraction pattern resembles that of phase **I**, as was calculated from the structure data of single-crystal diffraction at 298 K, except for the small discrepancies in the refined lattice parameters (a = 15.921(5) Å, b = 11.045(4) Å, c = 14.364(3) Å, β = 118.08(1)°). The diffraction patterns at other temperatures down to 230 K are essentially the same with slight shifts of diffraction lines due to the cell contraction. At 210 K, however, significant shifts of some reflections show that a structural change occurs. In particular, the peaks at 20.6 and 21.3° are shifted toward 20.8 and 21.7°, respectively, and that at 23.0° is shifted to 22.9° (indicated by asterisks in Figure 6).

Using the structural data obtained from single-crystal diffraction for phase **II**, a close resemblance is obtained between the observed and the calculated profiles with the refined lattice parameters a = 15.835 (5) Å, b = 10.720(4) Å, c = 43.82(1) Å, and β = 117.28(1)°. Therefore, this structural phase transition corresponds to the transition between phase **I** and phase **II**, and the transition temperature,

(16) Kahn, O.; Kröber, J.; Jay, C. *Adv. Mater.* **1992**, *4*, 718.
(17) Kröber, J.; Audière, J.-P.; Claude, R.; Codjovi, E.; Kahn, O.; Haasnoot, J. G.; Grolière, F.; Jay, C.; Bousseksou, A.; Linares, J.; Varret, F.; Gonthier-Vassal, A. *Chem. Mater.* **1994**, *6*, 1404.

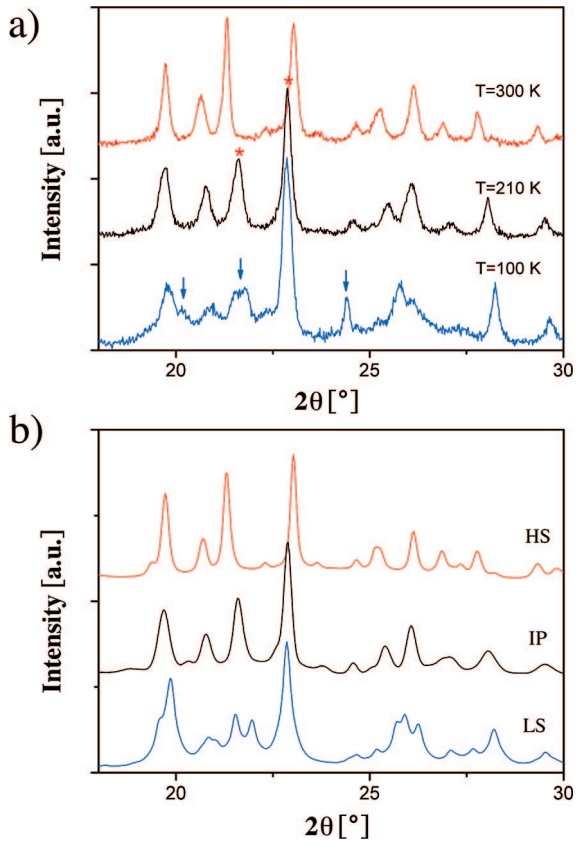

Figure 6. (a) Portion of powder X-ray diffraction patterns of compound **1** [sample (a)] showing the effects of cooling. The first structural change occurs between 230 and 210 K, which is characterized by significant shifts of the reflections at $2\theta \approx 20.6$, 21.3, and 23.0° (indicated by asterisks). The second transition takes place between 120 and 100 K, which can be seen by the appearance of reflections at, e.g., $2\theta \approx 20.1$ and 24.4° and the peak splittings at $2\theta \approx 21.7°$ (indicated by arrows). (b) Theoretical powder X-ray diffraction patterns of phases **I** (HS), **II** (IP), and **III** (LS) of compound **1**, as calculated from the single-crystal X-ray structures determined at 295 (red), 190 (black), and 110 K (blue), respectively.

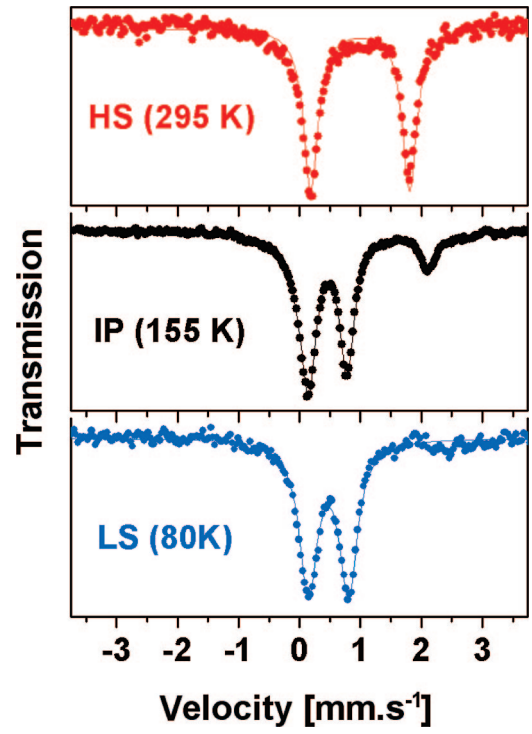

Figure 7. Mössbauer spectra at 295, 200, and 80 K [powder sample (a)].

observed between 230 and 210 K, is consistent with that measured by magnetic susceptibility measurements (221 K, see Table 1) and calorimetry (211 K, see Figure 3).

Upon further cooling sample (a), a second structural change is observed between 120 and 100 K, which is characterized by the appearance of some diffraction lines, for example, $2\theta \approx 20.1°$ and 24.4° and the peak splitting at 2θ around 21.6° (indicated by arrows in Figure 6). Again, the observed profiles show great similarity with the calculated one using the structural data of phase **III** and the lattice parameters $a = 15.807(11)$ Å, $b = 10.785(8)$ Å, $c = 14.229(7)$ Å, $\alpha = 91.41(3)°$, $\beta = 116.95(3)°$, and $\gamma = 89.61(4)°$. We concluded, therefore, that the second phase transition for sample (a) is the transition between phase **II** and phase **III**, as observed earlier on a single crystal,[6] though the apparent transition temperature is somewhat lower than that determined from the magnetic measurements.

^{57}Fe Mössbauer Spectroscopy. X-ray diffraction, whether performed on one single crystal or on a powder sample, is a long-range characterization technique giving the average unit cell over time and space. On the other hand, ^{57}Fe Mössbauer spectroscopy is a local sensitive probe that may provide rich information on the iron sites found within a macroscopic powder sample. Mössbauer spectra of a sample (a) of compound **1** were hence recorded at 265, 180, 155, and 80 K in the cooling mode and at 200 and 295 K in the heating mode, to check whether the characteristics of the iron sites fit with those observed from the X-ray diffraction data (see Figure 7 and fitting parameters in Table 4). Both high-temperature spectra (295 and 265 K, phase **I**) can be fitted with one doublet, the hyperfine parameters of which being characteristic for a single HS ($S = 2$) iron(II) site. The three spectra at intermediate temperatures (200, 180, and 155 K, phase **II**) display the wide plateau with one type of LS iron(II) and HS iron(II) sites at each temperature; about two-thirds (70%) of the iron centers have undergone the HS → LS transition. The spectrum at 80 K displays again only one doublet characteristic for a LS ($S = 0$) iron(II) species. These Mössbauer results corroborate nicely with those obtained from single-crystal X-ray diffraction and in particular the existence of one unique iron site in the phases **I** and **III**. On the other hand, it has to be noted that, as can be expected, the Mössbauer hyperfine parameters of the LS species are apparently not too sensitive to the small structural changes when going from phase **II** to **III** and therefore the Mössbauer spectrum of phase **II** appears as a mixture of the spectra of phase **I** and **III**.

Raman Spectroscopy. Similarly to Mössbauer spectroscopy, Raman spectroscopy is a local probe that provides a complementary view on the structural changes that are associated with the spin transition in compound **1**. One single crystal of compound **1** has been excited with a He−Ne laser (632.8 nm) at 303, 210, 130, and 77 K, and the corresponding Raman spectra have been recorded between 60 and 2250 cm^{-1} (see Figure 8).

Overall, the spectra at 303 K (phase **I**, HS) and 130 K (phase **III**, LS) are significantly different, with frequencies that are present for phase **I** (for instance, at 154, 207, 244,

Table 4. Mössbauer Parameters and Their Associated Standard Uncertainties for Compound 1 [Powder Sample (a)][a]

T [K]	δ (HS) [mm·s^{-1}]	ΔE_Q (HS) [mm·s^{-1}]	$\Gamma/2$ (HS) [mm·s^{-1}]	δ (LS) [mm·s^{-1}]	ΔE_Q (LS) [mm·s^{-1}]	$\Gamma/2$ (LS) [mm·s^{-1}]	A_{LS}/A_{tot} [%]
265	1.009(7)	1.70(1)	0.20(1)	n.o.	n.o.	n.o.	0
180	1.04(1)	2.07(3)	0.20(2)	0.466(6)	0.61(1)	0.148(7)	64(2)
155	1.061(9)	2.13(2)	0.21(2)	0.466(2)	0.626(4)	0.144(3)	73(1)
80	n.o.	n.o.	n.o.	0.474(4)	0.660(8)	0.179(6)	100
200	1.05(1)	1.96(2)	0.19(2)	0.462(5)	0.62(1)	0.150(6)	60(2)
295	0.995(5)	1.62(1)	0.166(8)	n.o.	n.o.	n.o.	0

[a] The first four spectra were recorded in the cooling mode and the last two spectra in the heating mode. δ, ΔE_Q, Γ, and A_{LS}/A_{tot} stand for the isomer shift, the quadrupole splitting, the half-height line width, and the relative area of the LS doublet, respectively; n.o. = not observed.

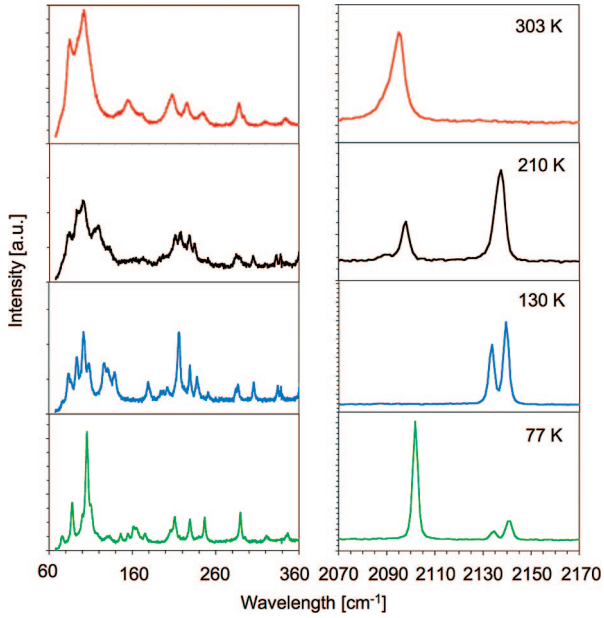

Figure 8. Raman spectra for compound **1** at 303, 210, 130, and 77 K (from top to bottom, respectively). Left: low wavenumber region (60−360 cm^{-1}). Right: thiocyanate stretching region (2070−2170 cm^{-1}).

686, 992, 1013, 1278 cm^{-1}) but not for phase **III**. At 210 K (phase **II**, IP), the spectrum between 400 and 2000 cm^{-1} corresponds mostly to the superimposition of the spectra of the HS and LS phases (see the Raman modes at 1326/1335 cm^{-1} and 1014/1027 cm^{-1}). However, this superimposition is not observed in the low (<400 cm^{-1}) and high (>2000 cm^{-1}) wavenumber regions, as shown in Figure 8.

The analysis of the low frequency region is difficult due to the large number of modes and the various couplings between them. However, it should be noted that changes occurring in this frequency region give the main contribution to the measured entropy change, which accompanies the two-phase transitions. In the high wavenumber region (2070−2170 cm^{-1}), for which the stretching modes of the thiocyanate ligands are found,[18] large differences are observed between the spectra of the three phases **I**, **II**, and **III**. In phase **I** (303 K), a single Raman active stretching mode is observed at 2096 cm^{-1}, which is consistent with two C_2-symmetric (i.e., in trans configuration) thiocyanate ligands of the HS compound, as observed by single-crystal X-ray diffraction.

In phase **II** (210 K), two modes are observed at 2098 and 2138 cm^{-1} in a ratio of approximately 1:2. These Raman modes are ascribed to a mixture of one HS and one LS iron centers in the sample at 210 K in approximately a 1:2 (HS/LS) proportion. Such observations are also consistent with the crystal structure of phase **II** at 190 K. In phase **III** (130 K), two well-resolved vibrational modes are observed at 2134 and 2139 cm^{-1} in the thiocyanate stretching region, which might correspond to the symmetric and antisymmetric modes of two nonequivalent thiocyanate ligands in the LS molecules, in agreement with the X-ray data at 110 K. It is important to underline that the Raman active vibration of the LS molecules in the IP is a single mode, whereas in the LS phase it is composed of two well-resolved modes. In other words, the Raman spectrum of the IP is not a simple mixture of the two pure (HS and LS) phases.

Light-Induced Excited State Spin Trapping. At 77 K under irradiation with the laser of the Raman spectrometer, the Raman spectrum of a single crystal of compound **1** is comparable to the spectrum recorded at 303 K (phase **I**), except that the peaks are in general much narrower and shift to slightly higher wavenumbers due to the large decrease in temperature (see Figure 8, bottom). At such low temperature only phase **III** should be thermodynamically stable according to single-crystal X-ray diffraction, Mössbauer, DSC, and magnetic measurements. The Raman spectrum at 77 K is hence indicative of a light-induced excited state spin trapping (LIESST)[14] of the HS phase by irradiation of a single crystal of **1** in the LS phase (phase **III**). In the thiocyanate stretching region, the intensities of the LS phase modes at 2135 and 2140 cm^{-1} become relatively small (∼25% of the total area), whereas an intense mode (∼75% of the total area) appears at 2102 cm^{-1} for the HS phase. Considering that the characteristic LS phase marker of the IP (phase **II**) is not observed at 2138 cm^{-1}, the spectrum at 77 K suggests that the light-induced HS phase corresponds to phase **I**, and not to phase **II**.

Although Raman spectroscopy clearly suggests the occurrence of the LIESST effect, we also undertook photomagnetic measurements to characterize the stability of the photoinduced metastable HS phase in the dark via the T(LIESST) method proposed by Létard et al.[19] A polycrystalline sample of compound **1** [type (b)] has been irradiated with an Ar$^+$ laser (457−514.5 nm) at 10 K in the SQUID magnetometer until saturation of the magnetization. Then, the laser was switched off and the sample was warmed up in the dark at a rate of +1.0(1) K·min^{-1}. The relaxation curve is shown in Figure 9.[20] Internal calibration enables that roughly 70% of the sample has been transformed in the HS phase after 2 h of irradiation to be calculated; the

(18) The IR-active thiocyanate stretching mode was also observed at room temperature around 2094 cm^{-1} by infrared spectroscopy on the powder.

(19) Létard, J. F.; Capes, L.; Chastanet, G.; Moliner, N.; Létard, S.; Real, J. A.; Kahn, O. *Chem. Phys. Lett.* **1999**, *313*, 115.

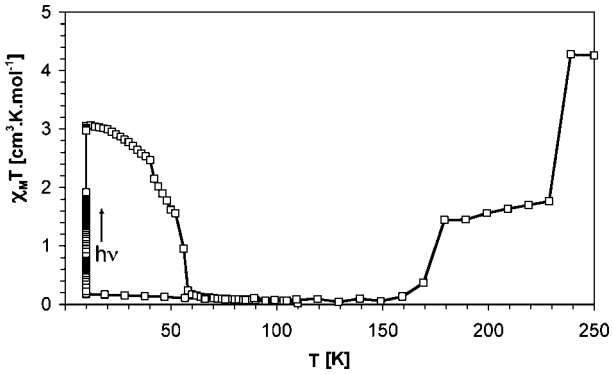

Figure 9. Variation of $\chi_M T$ of **1** [sample (b)] from 250 to 10 K, followed by light irradiation (2 h) at 10 K by a 10 mW Ar^+ laser (457−514.5 nm), then slow heating of the sample up to 100 K and cooling down to 10 K in the dark.

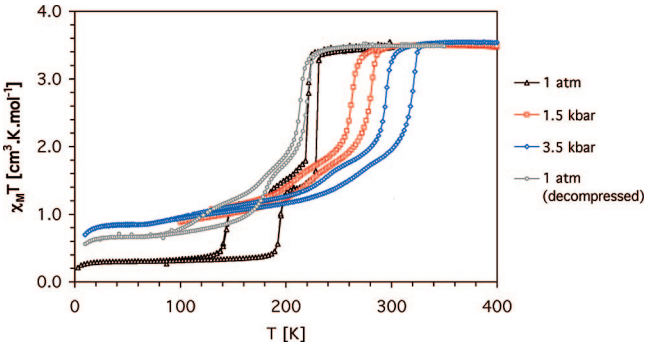

Figure 10. Effect of pressure on the magnetic behavior of compound **1** (powder). Cooling/heating rates: ± 1.0(1) K·min^{-1}.

minimum of the $d\chi_M T/dT$ versus T curve determines the T(LIESST) temperature, in this case 56 K.

Influence of Pressure. As a result of the large variations (∼0.2 Å) of the Fe−N distances and the concomitant volume change when the HS → LS spin transition occurs, the spin-crossover phenomenon is known to be sensitive to hydrostatic pressure.[21,22] In a first experiment, the magnetic susceptibility of a powder sample of compound **1** has been measured under 1.5 and 3.5 kbar hydrostatic pressure as a function of T to investigate the sensitivity of the solid material toward an increase of pressure. Then, the sample has been decompressed to atmospheric pressure and its magnetic behavior checked again. As depicted in Figure 10, major changes in the magnetic behavior are observed: (1) the temperature of the higher-temperature transition increases (see Table 5); (2) the hysteresis loop of the higher-temperature transition becomes broader (see Table 5); and (3) the lower-temperature transition is suppressed under pressure. This second transition is only partly recovered after decompression.

Table 5. Transition Temperatures and Hysteresis Widths of Compound 1 (Powder) under Pressure for the First Step of the Transition (Phase I to Phase II)

pressure (bar)	$T^1_c\downarrow$ (K)	$T^1_c\uparrow$ (K)	ΔT_{hyst} (K)
1	221(1)	231(1)	10(1)
1500	262(2)	280(2)	18(3)
3500	295(2)	320(2)	25(3)
1 (decompressed)	214(2)	220(2)	6(3)

Discussion

Influence of Sample Preparation and History on SCO. The properties of spin-crossover compounds in the solid state are known to be very sensitive to sample preparation.[1] Solvent inclusion,[5,23−33] mechanical grinding,[34−40] and polymorphism[28,41−45] must be inspected to ensure good reproducibility of the results. For instance, it has been known for many years that crystalline samples of the SCO compound $[Fe(phen)_2(NCS)_2]$ do not exhibit the same spin-transition properties as that of the precipitated material of the same chemical composition.[46] During the synthesis of compound **1**, a methanolic solution of $[Fe(NCS)_2]$ was added into a suspension of the bapbpy ligand.[47] Since both the bapbpy ligand and its Fe(II) compound **1** are insoluble in

(20) Note that the singularity in the relaxation curve around 40 K might indicate a two-step relaxation process, but its magnitude is comparable with the experimental incertitude.
(21) Gütlich, P.; Ksenofontov, V.; Gaspar, A. B. *Coord. Chem. Rev.* **2005**, *249*, 1811.
(22) Ksenofontov, V.; Gaspar, A. B.; Gütlich, P. *Top. Curr. Chem.* **2004**, *235*, 23.
(23) Gütlich, P.; Koppen, H.; Steinhauser, H. G. *Chem. Phys. Lett.* **1980**, *74*, 475.
(24) Sorai, M.; Ensling, J.; Hasselbach, K. M.; Gütlich, P. *Chem. Phys.* **1977**, *20*, 197.
(25) Hostettler, M.; Tornroos, K. W.; Chernyshov, D.; Vangdal, B.; Burgi, H. B. *Angew. Chem., Int. Ed.* **2004**, *43*, 4589.
(26) Gimenez-Lopez, M. C.; Clemente-Leon, M.; Coronado, E.; Romero, F. M.; Shova, S.; Tuchagues, J. P. *Eur. J. Inorg. Chem.* **2005**, 2783.
(27) Bartel, M.; Absmeier, A.; Jameson, G. N. L.; Werner, F.; Kato, K.; Takata, M.; Boca, R.; Hasegawa, M.; Mereiter, K.; Caneschi, A.; Linert, W. *Inorg. Chem.* **2007**, *46*, 4220.
(28) Neville, S. M.; Leita, B. A.; Offermann, D. A.; Duriska, M. B.; Moubaraki, B.; Chapman, K. W.; Halder, G. J.; Murray, K. S. *Eur. J. Inorg. Chem.* **2007**, 1073.
(29) Nihei, M.; Han, L. Q.; Oshio, H. *J. Am. Chem. Soc.* **2007**, *129*, 5312.
(30) Clemente-Leon, M.; Coronado, E.; Gimenez-Lopez, M. C.; Romero, F. M. *Inorg. Chem.* **2007**, *46*, 11266.
(31) Leita, B. A.; Neville, S. M.; Halder, G. J.; Moubaraki, B.; Kepert, C. J.; Letard, J. F.; Murray, K. S. *Inorg. Chem.* **2007**, *46*, 8784.
(32) Holland, J. M. *Dalton Trans.* **2002**, 548.
(33) Amoore, J. L. M.; Kepert, C. J.; Cashion, J. D.; Moubaraki, B.; Neville, S. M.; Murray, K. S. *Chem.-Eur. J.* **2006**, *12*, 8220.
(34) Müller, E. W.; Spiering, H.; Gütlich, P. *Chem. Phys. Lett.* **1982**, *93*, 567.
(35) Haddad, M. S.; Federer, W. D.; Lynch, M. W.; Hendrickson, D. N. *J. Am. Chem. Soc.* **1980**, *102*, 1468.
(36) Haddad, M. S.; Federer, W. D.; Lynch, M. W.; Hendrickson, D. N. *Inorg. Chem.* **1981**, *20*, 131.
(37) Miyazaki, Y.; Nakamoto, T.; Ikeuchi, S.; Saito, K.; Inaba, A.; Sorai, M.; Tojo, T.; Atake, T.; Matouzenko, G. S.; Zein, S.; Borshch, S. A. *J. Phys. Chem. B* **2007**, *111*, 12508.
(38) Ohshita, T.; Tsukamoto, A.; Senna, M. *Phys. Status Solidi A* **2004**, *201*, 762.
(39) Sorai, M.; Burriel, R.; Westrum, E. F.; Hendrickson, D. N. *J. Phys. Chem. B* **2008**, *112*, 4344.
(40) Weber, B.; Kaps, E. S.; Desplanches, C.; Letard, J. F. *Eur. J. Inorg. Chem.* **2008**, 2963.
(41) Galet, A.; Munoz, M. C.; Gaspar, A. B.; Real, J. A. *Inorg. Chem.* **2005**, *44*, 8749.
(42) Gaspar, A. B.; Munoz, M. C.; Moliner, N.; Ksenofontov, V.; Levchenko, G.; Gütlich, P.; Real, J. A. *Monatsh. Chem.* **2003**, *134*, 285.
(43) Matouzenko, G. S.; Bousseksou, A.; Lecocq, S.; van Koningsbruggen, P. J.; Perrin, M.; Kahn, O.; Collet, A. *Inorg. Chem.* **1997**, *36*, 5869.
(44) Reger, D. L.; Gardinier, J. R.; Smith, M. D.; Shahin, A. M.; Long, G. J.; Rebbouh, L.; Grandjean, F. *Inorg. Chem.* **2005**, *44*, 1852.
(45) Rajadurai, C.; Qu, Z. R.; Fuhr, O.; Gopalan, B.; Kruk, R.; Ghafari, M.; Ruben, M. *Dalton Trans.* **2007**, 3531.
(46) König, E.; Madeja, K. *Inorg. Chem.* **1967**, *6*, 48.
(47) The synthesis is done in presence of traces of ascorbic acid to avoid aerial oxidation of Fe(II) into Fe(III), although it can also be performed under an inert atmosphere, for which ascorbic acid is not required.

methanol the metalation of the ligand takes place in a heterogeneous system: the undissolved bapbpy ligand is little by little impregnated with dissolved [Fe(NCS)$_2$].

The phase-transition temperatures measured for compound **1** on the crude powder [sample (a)] or on the recrystallized material [sample (b)] are different (see Figures 2 and 3). As the cooling and heating rates are the same for both types of samples, such differences might result from slightly different chemical compositions or impurities and other kind of defects in the crystal lattice that cannot be detected by powder X-ray diffraction due to the low sensitivity of this technique.[48] Traces of impurities in sample (a) could explain the inconsistent elemental analysis of the crude powder (typically, a good fit to the calculated value would require 0.5 molecule of H_2O or methanol). As sample (b) is recrystallized and no solvent molecule is inserted in the crystal lattice, the purity of sample (b) is likely to be higher than that of sample (a). However, magnetic susceptibility measurements, powder X-ray diffraction, Mössbauer spectroscopy, and DSC all indicate that the magnetic behavior of the crude powder [sample (a)] has similar characteristics as that of the crystalline form [samples (b)], since it is characterized by two steps, two hysteresis loops, and two steep transitions.

It is well-known that intermolecular interactions like H-bonding and $\pi-\pi$ stacking can play an important role in the cooperativity of SCO materials.[49] The difference in cooperativity but also in transition temperature between compounds **1** and **2** can be rationalized by comparisons of their crystal structure details. First, the transition temperature for compound **2** is significantly lower than for compound **1** (see Table 1), which implies that the ligand-field strength for the former is weaker than for the latter. This might be the result of the bending of the thiocyanate ions with respect to the N4−Fe1−N8 axis, which can be observed in the crystal structure of **2** at 150 K (HS state): the Fe1−N4−S1 and Fe1−N8−S2 angles are lower than 160° (see Table 3). In contrast, the corresponding angles for the HS state of compound **1** are 170.66° (Fe1−N4−S1, phase **I**) and 168.74° (Fe2−N4B-S1B, phase **II**), which allows better coordination, that is, a stronger ligand field. Some of us recently published similar observations.[50]

Second, the presence of DMF molecules acting as hydrogen-bond acceptors in the crystal structure of **2** contributes to the formation of the H-bonded motif {DMF···[Fe(bapbpy)(NCS)$_2$]···DMF}. Consequently, the N−H···S and $\pi-\pi$ stacking intermolecular interactions found along the *c* direction in phases **I**, **II**, and **III** of compound **1** do no longer exist in the crystal structure of compound **2**. Such changes in intermolecular interactions may contribute to the lack of cooperativity of the SCO in compound **2** (see Figure 2). However, compound **2** remains a spin-crossover compound, showing that the ligand field created by the bapbpy and the two thiocyanate ligands leads to a favorable situation for the occurrence of an SCO. Therefore, the [Fe(bapbpy)(NCS)$_2$] unit may be seen as a starting building block for multifunctional spin-transition systems.[51]

The influence of sample history on the magnetic behavior of SCO compounds has previously been reported. In many cases, the crystallinity of a SCO material is lost during cooling and/or heating, thus hampering the structure determination by X-ray diffraction for some phases. In a demonstrative example, Miyazaki et al. recently reported that crystals of [Fe(dapp)(abpt)](ClO$_4$)$_2$ (dapp = bis(3-aminopropyl)(2-pyridylmethyl)amine, abpt = 4-amino-3,5-bis(pyridin-2-yl)-1,2,4-triazole) become fragmented whenever the crystals undergo the spin transition, which has been regarded as a self-grinding effect.[37] In other examples,[52−54] the two-step SCO properties change upon repeating the HS → LS → HS cycles, and the original behavior is restored after the sample has been allowed to rest. In the case of compound **1**, the repetition of the HS → LS → HS cycles up to six times did not modify significantly its SCO properties (e.g., transition temperatures, width of hysteresis), neither in the powder nor in the polycrystalline form.[55] In addition, by determining the single-crystal X-ray structures of the three phases and by studying the variations of the cell parameters with the temperature, we have shown in our previous communication that there was no significant loss of crystallinity when the crystals undergo the spin transitions in both cooling and heating modes.[6] In conclusion, there is no significant crystal damage as **1** undergoes spin transitions.

Nature of the IP and Comparison with Other Two-Step SCO Systems. We previously reported that phases **I** (HS), **II** (IP), and **III** (LS) of compound **1** have very similar crystal packing.[6] According to Herbstein's review about the mechanism of some first-order solid−solid phase transition,[9] compound **1** can be regarded as a polymorphic system with two reversible first-order single-crystal-to-single-crystal phase transitions and one ordered IP (i.e., phase **II**). Extra Bragg reflections, which do not result from the superimposition of the diffraction patterns of phases **I** and **III**, are found at temperatures for which phase **II** is stable. Complementarily, Raman spectroscopy gives a signature for phase **II** that is different from the superimposition of the spectra of phases **I** and **III**. We conclude that phase **II** is not a mixture of phases **I** and **III** but rather a new phase.

For two-step SCO compounds, an "IP" is defined as a new phase (i.e., crystallographically distinguishable from the HS and LS phases) that is thermodynamically stable at intermediate temperatures.[9] Until recently, the origin of two steps for mononuclear SCO complexes has been attributed to the

(48) The infrared spectrum of various samples of type (a) are always identical to that of crushed single crystals of **1** [i.e., sample (b) after grinding], and their powder X-ray diffraction spectrum at room temperature (Figure 6) fits well with the spectrum calculated for phase **I**.

(49) Bousseksou, A.; Salmon, L.; Varret, F.; Tuchagues, J. P. *Chem. Phys. Lett.* **1998**, *282*, 209.

(50) Sanchez Costa, J.; Lappalainen, K.; de Ruiter, G.; Quesada, M.; Tang, J.; Mutikainen, I.; Turpeinen, U.; Grunert, M.; Gütlich, P.; Lazar, H. Z.; Létard, J.-F.; Gamez, P.; Reedijk, J. *Inorg. Chem.* **2007**, *46*, 4079.

(51) Gaspar, A. B.; Ksenofontov, V.; Seredyuk, M.; Gütlich, P. *Coord. Chem. Rev.* **2005**, *249*, 2661.

(52) Guionneau, P.; Le Gac, F.; Kaiba, A.; Sanchez Costa, J.; Chasseau, D.; Létard, J.-F. *Chem. Commun.* **2007**, 3723.

(53) Grunert, C. M. *J. Phys. Chem. B* **2007**, *111*, 6738.

(54) Bhattacharjee, A.; Ksenofontov, V.; Sugiyarto, K. H.; Goodwin, H. A.; Gütlich, P. *Adv. Funct. Mater.* **2003**, *13*, 877.

(55) The small variations of $\chi_M T$ in the HS phase after each cycle (as shown in Figure 5) can be interpreted as a small displacement of the loosely packed crystals in the sampler holder until the most stable arrangement is attained.

presence of two crystallographically nonequivalent iron(II) sites in the unit cell of the HS phase, which undergo their spin transition at two different temperatures. In the past decade, a few mononuclear two-step SCO complexes have been reported where the HS phase has only one crystallographic iron(II) site.[7,31,56,57] For some of them, the IP is a 1:1 mixture of the HS and LS phases; the Fe−N distances measured by X-ray diffraction in the IP are intermediate (typically 2.1 Å) between that of a HS (≈2.2 Å) and that of a LS (≈2.0 Å) iron(II) center.[31,56] For $[Fe(2\text{-pic})_3]Cl_2 \cdot EtOH$ (2-pic = 2-picolylamine) the two-step spin transition is complete at low temperatures and the IP is a new ordered phase:[7,58] it is made of [HS···LS] dimers, and two sets of Fe−N bond distances can be measured, one for the LS centers and one for the HS centers. $(Fe[HC(3,5\text{-}Me_2pz)_3]_2)(BF4)_2$[57,59] (pz = pyrazolyl ring) has also one single crystallographic site in the HS phase and an ordered HS/LS IP below 206 K; however, the spin transition of the second half of the iron sites does not take place down to 5 K, and the LS phase has not been yet described. In all these compounds the HS/LS ratio in the IP is 1:1.

For compound **1**, the results obtained from magnetic measurements, Mössbauer and Raman spectroscopies, and powder and single crystal X-ray diffraction techniques are altogether consistent: (i) **1** has only one iron(II) site in the HS and LS phases; (ii) the HS/LS ratio in the IP is 1:2; (iii) its IP is stable over a wide temperature range; and (iv) there are no solvent molecules in the crystal lattice. To our knowledge, such a combination of characteristics had not been described yet. Two-step iron(II) SCO compounds with an IP in which the HS/LS ratio is 1:2 are scarce. In $[Fe(isoxazole)_6](BF_4)_2$,[60] the single-crystal X-ray structure of the HS phase shows two crystallographically independent HS Fe(II) sites, one of which accounts for 1/3 of the Fe(II) centers and remains in the HS state over the whole temperature range.[61] For the second site, which accounts for 2/3 of the Fe(II) centers, two slightly different coordination environments are observed by Mössbauer spectroscopy in a 1:1 ratio;[60] they undergo spin transitions at two different temperatures separated by about 100 K. The X-ray structure of the LS phase has not been reported yet. In $[Fe(etz)_6](BF_4)_2$ (etz = 1-ethyl-1*H*-tetrazole) two crystallographically inequivalent iron(II) centers A and B are found in a 2:1 ratio at high temperatures, of which only the former undergoes a single-step spin transition.[62] Hence at low temperatures the LS/HS ratio is 2:1.

Several models have been proposed to explain the occurrence of two-step SCO, which all account for a 1:1 HS/LS ratio in the IP.[58,63−68] In particular, the [HS···HS] ↔ [HS···LS] ↔ [LS···LS] symmetry-broken phase transition of $[Fe(2\text{-pic})_3]Cl_2 \cdot EtOH$ has been modeled soon after the observation of the [HS···LS] IP of this compound.[69] The existence of the IP is seen as a result of competitive effects between local (antiferromagnetic-like intradimer coupling) and long-range elastic interactions. Similar ideas have been proposed in the case of the dinuclear compound $\{[Fe(bt)(NCS)_2]_2(bpym)\}$ (bt = 2,2′-bithiazoline; bpym = 2,2′-bipyrimidine).[70] For $[Fe(2\text{-pic})_3]Cl_2 \cdot EtOH$ a relationship between the disorder of the EtOH molecules as the temperature increases and the easiness with which the Fe(II) centers can change from LS to HS states is assumed.[69] Indeed, experimentally the two successive order−disorder transitions coincide with the two steps in the spin-transition curve.[7] In compound **1**, there are no lattice solvent molecules in the crystal structures and the three phases are ordered. Additionally, the two steps in **1** correspond to two first-order phase transitions, which has been observed previously only in the case of the compound $\{Fe[5\text{-}NO_2\text{-sal-}N(1,4,7,10)]\}$.[71,72] The phase sequence **I** ↔ **II** ↔ **III** is characterized by the repetitive motif [···HS···] ↔ [···LS···HS···LS···] ↔ [···LS···], which is found along the crystallographic *c* axis. This new example needs further theoretical studies to be fully understood.

As a first step for the interpretation of the two-step SCO behavior and the peculiar stability of the [LS···HS···LS] IP observed in **1**, the Ising-like Hamiltonian described in ref 64 can be adapted to the particular situation of the present compound: three sublattices with the same energy gap Δ between the HS and LS states (in agreement with the structural study) and three different interactions (J_{AB}, J_{BC}, J_{AC}). The origin of the difference between the interactions is obviously due to the existence of different short- and long-range elastic interactions in the crystal network. The one-site Hamiltonian of the system can be written in the mean field approximation as follows:

$$\mathcal{H} = \mathcal{H}_A + \mathcal{H}_B + \mathcal{H}_C$$

with

$$\mathcal{H}_A = \Delta/2\sigma_A + J_{AB}\sigma_A\langle\sigma_B\rangle + J_{AC}\sigma_A\langle\sigma_C\rangle$$
$$\mathcal{H}_B = \Delta/2\sigma_B + J_{AB}\sigma_B\langle\sigma_A\rangle + J_{BC}\sigma_B\langle\sigma_C\rangle$$
$$\mathcal{H}_C = \Delta/2\sigma_C + J_{BC}\sigma_C\langle\sigma_B\rangle + J_{AC}\sigma_C\langle\sigma_A\rangle$$

where $\sigma_{A,B,C}$ are the fictious spins with the eigenvalues +1 for the HS state and −1 for the LS state. The high-spin

(56) Matouzenko, G. S.; Luneau, D.; Molnar, G.; Ould-Moussa, N.; Zein, S.; Borshch, S. A.; Bousseksou, A.; Averseng, F. *Eur. J. Inorg. Chem.* **2006**, 2671.
(57) Reger, D. L.; Little, C. A.; Rheingold, A. L.; Lam, M.; Concolino, T.; Mohan, A.; Long, G. J. *Inorg. Chem.* **2000**, *39*, 4674.
(58) Chernyshov, D.; Burgi, H. B.; Hostettler, M.; Törnroos, K. W. *Phys. Rev. B* **2004**, *70*, 094116.
(59) Reger, D. L.; Little, C. A.; Young, V. G.; Maren, P. *Inorg. Chem.* **2001**, *40*, 2870.
(60) Bhattacharjee, A.; van Koningsbruggen, P. J.; Hibbs, W.; Miller, J. S.; Gütlich, P. *J. Phys.: Condens. Matter* **2007**, 19.
(61) Hibbs, W.; van Koningsbruggen, P. J.; Arif, A. M.; Shum, W. W.; Miller, J. S. *Inorg. Chem.* **2003**, *42*, 5645.
(62) Hinek, R.; Spiering, H.; Schollmeyer, D.; Gutlich, P.; Hauser, A. *Chem.-Eur. J.* **1996**, *2*, 1427.
(63) Huby, N.; Guerin, L.; Collet, E.; Toupet, L.; Ameline, J. C.; Cailleau, H.; Roisnel, T.; Tayagaki, T.; Tanaka, K. *Phys. Rev. B* **2004**, *69*, 020101.
(64) Bousseksou, A.; Nasser, J.; Linares, J.; Boukheddaden, K.; Varret, F. *J. Phys. I France* **1992**, *2*, 1381.
(65) Romstedt, H.; Spiering, H.; Gütlich, P. *J. Phys. Chem. Solids* **1998**, *59*, 1353.
(66) Koudriavtsev, A. B. *Monatsh. Chem.* **2006**, *137*, 1283.
(67) Boukheddaden, K.; Linares, J.; Codjovi, E.; Varret, F.; Niel, V.; Real, J. A. *J. Appl. Phys.* **2003**, *93*, 7103.
(68) Bolvin, H. *Chem. Phys.* **1996**, *211*, 101.
(69) Luty, T.; Yonemitsu, K. *J. Phys. Soc. Jpn.* **2004**, *73*, 1237.
(70) Ould-Moussa, N.; Trzop, E.; Mouri, S.; Zein, S.; Molnár, G.; Gaspar, A. B.; Collet, E.; Buron-Le Cointe, M.; Real, J. A.; Borshch, S.; Tanaka, K.; Cailleau, H.; Bousseksou, A. *Phys. Rev. B* **2007**, *75*, 054101.
(71) Boinnard, D.; Bousseksou, A.; Dworkin, A.; Savariault, J. M.; Varret, F.; Tuchagues, J. P. *Inorg. Chem.* **1994**, *33*, 271.
(72) Petrouleas, V.; Tuchagues, J. P. *Chem. Phys. Lett.* **1987**, *137*, 21.

fraction for each temperature is obtained as a function of the mean values of the operators σ_A, σ_B, and σ_C:

$$n_{HS} = 1/6(\langle\sigma_A\rangle + \langle\sigma_B\rangle + \langle\sigma_C\rangle) + 1/2$$

It is worth noticing that this Hamiltonian is similar to the Hamiltonian of dinuclear spin-crossover systems already studied in ref 64, where the main ingredient for the existence of the two-step SCO is the intramolecular interaction with different value (or with opposite sign) than the intermolecular interactions. In the framework of the above three sublattice Hamiltonians the two-step behavior can be obtained if $J_{BC} \neq J_{AB} = J_{AC}$. Clearly, this new Hamiltonian contains the main components to reproduce the two-step spin-crossover behavior observed in **1**. The detailed analysis of this model will be published elsewhere.

About the Phase Sequence I ↔ II ↔ III. The change in molecular symmetry for **1** has been examined in the phase sequence **I** ↔ **II** ↔ **III**. In phases **I** and **II**, all HS molecules adopt a C_2 symmetry and are located at sites of two-fold axial symmetry. In phases **II** and **III**, the LS molecules do not have the C_2 symmetry and are found at no special position. The Z' variations[73] 1/2 ↔ 1 + 1/2 ↔ 1 in the sequence **I** ↔ **II** ↔ **III** result from changes in the molecular symmetry of **1** between room temperature and 110 K. As the transition **I** → **II** takes place, the crystal-lattice symmetry remains the same although 2/3 of the Fe centers undergo the HS → LS transition. The loss of crystal-lattice symmetry occurs after completion of the transition **II** → **III**, which is accompanied by the loss of the C_2 symmetry for all molecules of **1**. The HS → LS transition in (Fe[$H_2B(pz)_2$]$_2$phen), for which no IP was found, is also accompanied by the loss of C_2 molecular symmetry.[74]

The change in molecular symmetry observed through the phase sequence **I** ↔ **II** ↔ **III** could not take place without any significant structural changes. These largest changes are observed along [001]. In the three phases, the N−H···S hydrogen bonds and $\pi-\pi$ stacking interactions found between adjacent molecules of **1** along [001] contribute to the building of 1-D chains. In phase **I**, these chains are built of HS···HS contacts and the Fe···Fe separation distances are 7.1395(3) Å. In the IP **II**, the motif [LS···HS···LS] is found, and there are two HS···LS contacts and one LS···LS contact over three adjacent contacts along [001]. The Fe···Fe separation distances are always found to be shorter for HS···LS contacts [7.0483(4) Å] than for LS···LS contacts [7.1427(5) Å]. In phase **III**, the 1-D chains are built successively by short and long LS···LS contacts, and the Fe···Fe separation distances are 6.9563(7) and 7.2130(7) Å. These differences in the metal···metal separation distances are quite subtle (see Figure 11), but they might contribute to the unusual stability of the [LS···HS···LS] IP.

Cooperative effects might also derive from the variation of the hydrogen bonding and $\pi-\pi$ stacking interactions along [001] when the spin transition occurs. In phase **I**, the N−H···S interactions are the weakest [N···S = 3.424(2) Å], but the $\pi-\pi$ interactions between adjacent pyridine rings are the strongest [Cg···Cg′ = 3.881(1) Å]; the HS···HS contacts are neither too short nor too long. In phase **II**, the hydrogen bonds do not significantly vary [N···S = 3.356(2)−3.390(2) Å], but the $\pi-\pi$ interactions are stronger for the short HS···LS contacts [Cg···Cg′ = 3.820(2)−3.908(1) Å] and weaker for the long LS···LS contacts [Cg···Cg′ = 4.021(2) Å]. Similar feature are noticed for phase **III**: the hydrogen bonds do not vary [N···S = 3.342(2)−3.367(2) Å], and the LS···LS contacts are minimized via strong $\pi-\pi$ interactions and vice versa [Cg···Cg′ = 3.844(1) Å for short LS···LS and 4.055(1) Å for long LS···LS]. The H bonding network in phase **III** is comparable to that of phase **II**. Overall, the best HS···LS interactions appear to be transmitted mostly via $\pi-\pi$ stacking.

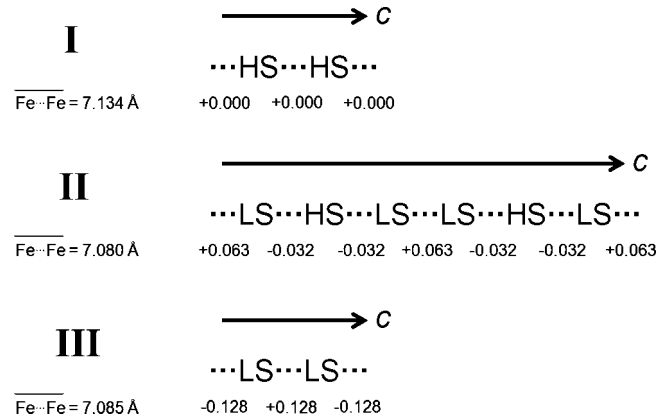

Figure 11. Drawing showing the different contact patterns in the three phases of **1** along [001]. The deviations (in Å) of the Fe···Fe distances from the average Fe···Fe distance calculated for each phase are indicated below all contacts. In phase **I**, the deviations are zero because all contacts are identical. In phase **II**, the distances are short for the LS···HS (and HS···LS) contacts but long for the LS···LS contacts. In phase **III**, the repetitive motif is made of a succession of short and long LS···LS contacts. In the phase sequence **I** ↔ **II** ↔ **III**, the $\Delta(Fe\cdots Fe)_{max-min}$ distances are zero for phase **I**, intermediate (∼0.10 Å) for phase **II**, and largest (∼0.26 Å) for phase **III**.

The existence of an IP with a HS/LS ratio of 1:2 might enable the minimization of the structural changes between contacts of adjacent molecules along the 1-D chains. The average Fe···Fe distance decreases by about 0.05 Å after completion of the transition **I** → **II**, and $\Delta(Fe\cdots Fe)_{max-min}$ in phase **II** is no larger than 0.10 Å. In phase **III**, the average Fe···Fe distance remains very similar to that found for phase **II**, but $\Delta(Fe\cdots Fe)_{max-min}$ has increased by a factor of about 2.5. The conversion of 100% of the iron(II) sites from the HS state to the LS state in one single step might be energetically unfavorable because the structural changes that would be required would be too large.

Influence of Light and Pressure. Light induced excited state spin trapping is one of the most interesting properties of SCO complexes.[10] Two different experiments at 10 K (photomagnetism) and at 77 K (Raman) show that the HS state of compound **1** can be optically populated by irradiation of the LS phase (phase **III**) with green or red light, respectively. Good optical conversions are reached in both cases (∼70−75%). The doubling of the laser power did not allow increasing the optical conversion but did lead to an increase of the temperature. As shown in Figure 9, a slow relaxation of the magnetization is observed between 10 and

(73) Z' = the number of formula units in the asymmetric unit.
(74) Thompson, A. L.; Goeta, A. E.; Real, J. A.; Galet, A.; Munoz, M. C. *Chem. Commun.* **2004**, 1390.

56 K (even at 10 K). In the Raman spectrometer the system is in the photostationary state, as the temperature is nearly 20 K above the *T*(LIESST) (56 K). The light-induced HS phase is likely to be phase **I** and not phase **II** since 70% LS → HS conversion is obtained in the photomagnetic experiment, while phase **II** contains only approximately 33% of HS ions. The Raman experiment is consistent with this finding, since the optically pumped material displays the spectral signature of phase **I** and (in smaller proportion) phase **III**, but no sign of phase **II** is detected. Concerning the relaxation process of the metastable HS phase it would be interesting to see whether it takes place in one step or via the IP, but this would require photocrystallographic measurements at liquid helium temperatures, which is beyond the scope of the present study.

Apart from light irradiation, hydrostatic pressure is also known to modify the spin-transition properties of SCO compounds.[21,75−77] Since LS species have a smaller volume/formula unit (i.e., *V*/*Z*) than HS species, an increase of the pressure is expected to favor the LS state, that is, the transition temperatures increase and, as a consequence, the hysteresis width decreases. These effects can be satisfactorily modeled within the frame of mean-field theory.[78−81] In the case of compound **1**, we observe an increase of the first transition temperature. The observed shift (ca. 23.4 K·kbar^{-1}) is somewhat different from what can be estimated using the Clausius−Clapeyron equation ($dT_c(p)/dp = \Delta V_{HL}/\Delta S_{HL}$ = 15.8 K·kbar^{-1}) on the basis of the available crystallographic and calorimetric data but falls in the typical range observed for SCO compounds with a $Fe^{II}N_6$ core.[82] On the other hand, the width of the first hysteresis cycle tends to increase with increasing pressure. This unusual phenomenon has already been observed in a few compounds and was explained in most cases by assuming the appearance of additional structural changes induced by the applied pressure.[22,83−85] The combined effects of pressure result in the hysteresis cycle falling into the technologically interesting room temperature range (at 3.5 kbar), where applications of compound **1** might thus be foreseen.[10,86] Even more surprisingly, the second transition seems to be suppressed under pressure, although the definitive proof of it would require additional X-ray diffraction studies under external pressure. After releasing the pressure of the powder sample, the second transition is recovered, although it is modified compared to the initial magnetic behavior of the powder (see Figure 10). The temperature dependence of the unit cell parameters shows that despite the volume per formula unit *V*/*Z* decreasing as crystals of compound **1** undergo the HS → IP and IP → LS transitions, there is a high anisotropy in the behavior of the cell parameters as crystals undergo the IP → LS transition: *a* does not vary significantly, whereas *b* decreases and *c* increases discontinuously at this transition.[6] The anisotropic effects may play a role in the pressure-dependent behavior: as the pressure is hydrostatic, the increase of *c* during the second transition may be unfavorable and hinder the second transition at high pressures. Additional X-ray studies under pressure are currently being undertaken to check these assertions.

Conclusions

In the present report, we discuss the influence of sample preparation, sample history, and physical conditions (temperature, light, pressure) on the recently discovered[6] mononuclear two-step SCO compound [Fe(bapbpy)$(NCS)_2$] (**1**). Overall, we have provided a thorough characterization of its HS, IP. and LS phases by single-crystal X-ray diffraction, powder X-ray diffraction, calorimetry, magnetic susceptibility measurements, Raman spectroscopy, Mössbauer spectroscopy, and optical microscopy. The observation of the high-temperature spin transition (HS ↔ IP) by optical microscopy reveals a transition front between large domains of mother and daughter phases (e.g., on cooling, phase **I** = mother phase and phase **II** = daughter phase) in a single crystal while the transition **I** ↔ **II** takes place. Although sample preparation is known to influence SCO, the difference in behavior between a crude and a recrystallized sample of compound **1** appears to be limited, as both types of samples show two-step SCO, steep transitions, and hysteresis loops. Our studies also illustrate that compound **1** is robust, as it is stable under air for months in the solid state and as there is no fatigue of the crystal lattice upon going repeatedly through the spin transitions. The solvated material [Fe(bapbpy)-$(NCS)_2$]·2DMF (**2**), which was obtained by varying the recrystallization conditions, is a single-step SCO compound that does not show any hysteresis. One-dimensional H-bonding networks appear to be critical for the cooperative behavior in compound **1**, as in **2** these infinite H-bonded networks are replaced by isolated {DMF···[Fe(bapbpy)-$(NCS)_2$]···DMF} units. The existence of an ordered IP with a 1:2 HS/LS ratio in compound **1** is unprecedented and is still difficult to rationalize, although we try to discuss it in terms of intermolecular HS···LS and LS···LS contacts in the crystal structure.

Irradiation of the LS phase (phase **III**) at low temperatures seems to generate the metastable HS phase (phase **I**) and not the IP (phase **II**); however, definitive proof of it would require X-ray diffraction experiments under light irradiation, which is beyond the scope of this article. We have also shown that applying hydrostatic pressure not only gives rise to the shifting of the high-temperature spin transition toward higher temperatures associated with the broadening of its hysteresis

(75) Boillot, M. L.; Zarembowitch, J.; Itie, J. P.; Polian, A.; Bourdet, E.; Haasnot, J. P. *New J. Chem.* **2002**, *26*, 313.
(76) Guionneau, P.; Brigouleix, C.; Barrans, Y.; Goeta, A. E.; Letard, J. F.; Howard, J. A. K.; Gaultier, J.; Chasseau, D. *C. R. Acad. Sci., Ser. II C* **2001**, *4*, 161.
(77) Bonhommeau, S.; Molnár, G.; Goiran, M.; Boukheddaden, K.; Bousseksou, A. *Phys. Rev. B* **2006**, *74*, 064424.
(78) Slichter, C. P.; Drickamer, H. G. *J. Chem. Phys.* **1971**, *56*, 2142.
(79) Adler, P.; Wiehl, L.; Meissner, E.; Kohler, C. P.; Spiering, H.; Gütlich, P. *J. Phys. Chem. Solids* **1987**, *48*, 517.
(80) Meissner, E.; Koppen, H.; Spiering, H.; Gütlich, P. *Chem. Phys. Lett.* **1983**, *95*, 163.
(81) Spiering, H.; Meissner, E.; Koppen, H.; Müller, E. W.; Gütlich, P. *Chem. Phys.* **1982**, *68*, 65.
(82) ΔV_{HL} = 18.9 Å^3·molecule^{-1}; ΔS_{HL} = 72 J·K^{-1}·mol^{-1} at 235 K.
(83) König, E.; Ritter, G.; Waigel, J.; Goodwin, H. A. *J. Chem. Phys.* **1985**, *83*, 3055.
(84) Ksenofontov, V.; Spiering, H.; Schreiner, A.; Levchenko, G.; Goodwin, H. A.; Gütlich, P. *J. Phys. Chem. Solids* **1999**, *60*, 393.
(85) Ksenofontov, V.; Levchenko, G.; Spiering, H.; Gütlich, P.; Letard, J. F.; Bouhedja, Y.; Kahn, O. *Chem. Phys. Lett.* **1998**, *294*, 545.
(86) Kahn, O.; Martinez, C. J. *Science* **1998**, *279*, 44.

loop but also seems to suppress the low-temperature spin transition (IP ↔ LS). Although anisotropy during the low-temperature transition is clearly evidenced and might rationalize such unusual behavior, X-ray studies under pressure are required to definitively prove these assumptions. Investigations are currently carried out to tackle these issues.

Experimental Part

Infrared spectra were measured on a Perkin-Elmer PARAGON 1000 FT-IR spectrometer equipped with a diamond ATR device. Powder X-ray diffraction data were collected on a Philips X'Pert PRO diffractometer equipped with the X'celerator using Cu Kα radiations. For low temperature X-ray diffraction, an Anton Paar TTK 450 chamber with the direct sample cooling/heating in the temperature range between 190 and 300 K and a temperature stability of <0.2 K was used.

Sample Preparation. Compound **1** was prepared as a powder [sample (a)] or recrystallized from DMF/methanol [samples (b) and (c)] according to the literature procedure.[6]

Compound **2** [sample (c)] was obtained by slow vapor diffusion of diisopropylether into a DMF solution of **1**: 50 mg of **1** (powder) was dissolved in 10 mL of degassed DMF under argon and stirred for 30 min. Two milligrams of ascorbic acid were added, and the solution was stirred for 5 min. Two milliliters of this solution were transferred via a syringe into one of the compartments of an H-tube containing, in the other compartment, 15 mL of degassed diisopropylether under argon. After 7 days of vapor diffusion under argon, dark single crystals of **2** appeared. They were filtered over Micropore Whatman filter paper (RC 55, pore Ø 0.45 μm), washed with MeOH (3 × 5 mL), and dried under vacuum ($P \approx 10^{-2}$ torr) at room temperature for 3 h. Yield: 8 mg of **2**. IR (298 K): 3312.9, 3205.1, 3079.5, 3039.8, 2928.0, 2874.7, 2061.3 (NCS), 1661.7 (DMF), 1651.8 (DMF), 1645.5 (DMF), 1635.3, 1576.0, 1537.9, 1482.8, 1462.9, 1456.5, 1435.9, 1428.0, 1386.4, 1367.5, 1243.3, 1228.7, 1173.5, 1158.6, 1134.6, 1100.7, 1057.7, 1007.3, 868.0, 797.7, 770.4, 681.8, 667.6, 645.2, 613.5, 516.1, 417.8, 355.9, 343.9, 328.8, 322.4 cm^{-1}. C, H, N: 50.41/3.39/21.48% (exp); 51.57/3.15/21.87% (calc).

Magnetic Susceptibility Measurements. A total of 6.30 mg of powder **1** [sample (a)], 4.87 mg of recrystallized **1** [sample (b)], or 6.01 mg of recrystallized **2** [sample (c)] were introduced in a sample holder which was mounted on a plastic straw before introduction in a Quantum Design MPMS-XL squid magnetometer. DC magnetization measurements were performed in a field of 0.5 T, from 300 to 3 K (cooling mode) and from 3 to 300 K (heating mode). The total measuring time was 20 h (cooling/heating rate: 1.0(1) K·min^{-1}). Corrections for the diamagnetism of the sample holder were calculated using Pascal's constants. For the sample history study the cooling/heating cycle was repeated six times on sample (b) with different cooling/heating rates: −1.01, −0.92, −0.83, −0.71, −1.08, and −0.66 K·min^{-1} (cooling mode); 1.05, 0.92, 0.84, 0.73, 1.12, and 0.68 K·min^{-1} (heating mode) for cycles 1−6, respectively.

Magnetic susceptibility measurements at high pressures were carried out in a magnetic field of 2 T at heating and cooling rates of 1 K·min^{-1} using a clamp-type, hardened beryllium bronze (CuBe) cell. Hydrostatic conditions are obtained by mixing the powder samples with a pressure transmitting mineral oil. Details of the pressure cell have been published previously.[87] Photomagnetic measurements were performed on a thin layer of polycrystalline compound using an Ar$^+$ laser (457.0−514.5 nm) and a sample rod allowing irradiation of the sample in the magnetometer via fiber optics.

Calorimetry. DSC measurements were carried out on 8.5 mg of powdered **1** [sample (a)] or 11.2 mg of recrystallized **1** [sample (b)] using a Netzsch DSC 204 instrument under helium purging gas (20 cm^3·min^{-1}) at a scan rate of 10 K min^{-1} in both heating and cooling modes. Temperature and enthalpy (ΔH) were calibrated using the melting transition of standard materials (Hg, In, Sn). The uncertainty in the transition enthalpy (ΔH) and entropy (ΔS) is estimated to be approximately 10% due to the subtraction of the unknown baseline and uncertainties in the residual (i.e., nontransformed) fractions. The calculated enthalpy/entropy changes are given per metal ion involved in each step of the transition.

^{57}Fe Mössbauer Measurements. ^{57}Fe Mössbauer measurements were carried out on sample (a) in a flow-type liquid nitrogen cryostat using a conventional constant acceleration type Mössbauer spectrometer. γ-rays were provided by a ^{57}Co(Rh) source (ca. 20 mCi). The spectrum evaluations were done with the assumption of Lorentzian line shapes using the Recoil software [http://www.isapp-s.ca/recoil/]. All isomer shifts are given relative to α-Fe at room temperature.

Raman Spectroscopy. Variable temperature Raman spectra were collected using a single-stage LabRAM-HR (Jobin Yvon) Raman spectrometer equipped with a He−Ne laser (632.8 nm). Samples were enclosed under nitrogen atmosphere on the coldfinger of a THMS600 (Linkam) liquid nitrogen cryostat.

X-ray Crystallography for 2. All reflection intensities were measured at 150(2) K using a Nonius Kappa CCD diffractometer (rotating anode) with graphite-monochromated Mo Kα radiation (λ = 0.71073 Å) under the program COLLECT.[88] The program PEAKREF[89] was used to refine the cell dimensions. Data reduction was done using the program EVALCCD.[90] The structure was solved with the program DIRDIF08[91] and was refined on F^2 with SHELXL-97.[92] Multiscan absorption corrections based on symmetry-related measurements were applied to the data with the program SADABS.[93] The temperature of the data collection was controlled using the system OXFORD CRYOSTREAM 600 (manufactured by OXFORD CRYOSYSTEMS). The H-atoms were placed at calculated positions (except when specified) using the instructions AFIX 43 or AFIX 137 with isotropic displacement parameters having values 1.2 or 1.5 times U_{eq} of the attached C atom. The H-atoms H2A and H6 located respectively on N2 and N6 were found from the difference Fourier map. The N−H bond distances were restrained to be 0.88 Å using the DFIX instruction. Illustrations were made with the program Mercury.[94] Structure validation was done with the program PLATON.[95]

The single crystal that was mounted on the diffractometer was found to be nonmerohedrally twinned. After determination of the cell dimensions, the program DIRAX[96] failed to identify the twinning, probably because the contribution of the minor twin

(87) Molnár, G.; Guillon, T.; Ould-Moussa, N.; Rechignat, L.; Kitazawa, T.; Nardone, M.; Bousseksou, A. *Chem. Phys. Lett.* **2006**, *423*, 152.
(88) Nonius. *COLLECT*; Nonius BV, Delft, The Netherlands, 1999.
(89) Schreurs, A. M. M. *PEAKREF*; Utrecht University: Utrecht, The Netherlands, 2005.
(90) Duisenberg, A. J. M.; Kroon-Batenburg, L. M. J.; Schreurs, A. M. M. *J. Appl. Crystallogr.* **2003**, *36*, 220.
(91) Beurskens, P. T.; Beurskens, G.; de Gelder, R.; Garcia-Granda, S.; Gould, R. O.; Smith, J. M. M. *The DIRDIF2008 program system*; Crystallography Laboratory, University of Nijmegen: Nijmegen, The Netherlands, 2008.
(92) Sheldrick, G. M. *Acta Crystallogr., Sect. A* **2008**, *64*, 112.
(93) Sheldrick, G. M. *SADABS 2006/1*; University of Göttingen: Göttingen, Germany, 2006.
(94) Macrae, C. F.; Edgington, P. R.; McCabe, P.; Pidcock, E.; Shields, G. P.; Taylor, R.; Towler, M.; van de Streek, J. *J. Appl. Crystallogr.* **2006**, *39*, 453.
(95) Spek, A. L. *J. Appl. Crystallogr.* **2003**, *36*, 7.

domain was too small to be detected. After a complete data set was collected, the reciprocal lattice slices were reconstructed using the program PRECESSION.[97] Extra spots were detected on the slices reconstructed down the a^* and b^* directions. The twinning was examined using the program TwinRotMat,[95] which found that the two twin domains are related by a twofold axis along the c^* direction. The fractional contribution of the minor twin component (i.e., the BASF batch scale factor) was refined to 0.0443(9).

Acknowledgment. We kindly acknowledge the COST Action D35/0011 and coordination by the FP6 Network of Excellence "Magmanet" (Contract No. 515767). This research has been financially supported by the Council for Chemical Sciences of The Netherlands Organization for Scientific Research (CW-NWO) and by the ANR project SCOOP (jeunes chercheurs).

Supporting Information Available: Movies of the transition between phases **I** and **II** of a single crystal of **1**, observed via optical microscopy in the cooling mode and in the heating mode (AVI format, cf. Figure 1). Crystallographic data in CIF format (X-ray structure of compound **2**). This material is available free of charge via the Internet at http://pubs.acs.org.

CM803414Q

(96) Duisenberg, A. J. M. *J. Appl. Crystallogr.* **1992**, *25*, 92.
(97) Nonius. *PRECESSION*; Nonius BV, Delft, The Netherlands: 1999.